EVALUATING THE LATTICE BOLTZMANN METHOD FOR LARGE EDDY SIMULATION WITH DYNAMIC SUB-GRID SCALE MODELS

Christos Gkoudesnes

Aerodynamics and Fluid Mechanics Research Group
Engineering and Physical Sciences Faculty
University of Southampton
Highfield Campus, Southampton SO17 1BJ, UK
C.Gkoudesnes@soton.ac.uk

Ralf Deiterding

Aerodynamics and Fluid Mechanics Research Group
Engineering and Physical Sciences Faculty
University of Southampton
Highfield Campus, Southampton SO17 1BJ, UK
R.Deiterding@soton.ac.uk

ABSTRACT

In this paper, we verify the newly implemented Large Eddy Simulation (LES) models, namely the Dynamic SMAgorinsky (DSMA) and the Wall-Adapting Local Eddy-viscosity (WALE) in our Lattice Boltzmann Method (LBM) solver. The test cases of Forced Homogeneous Isotropic Turbulence (FHIT) and Taylor Green Vortex (TGV) were employed for this purpose. Direct Numerical Simulations (DNS) of FHIT were carried out to establish a resolution criterion for LBM based on a model spectrum. The low dissipation behaviour of LBM was also confirmed by DNS of TGV. LES of both test cases were able to recover the expected DNS results and were used to measure the performance of the two models in question. Particularly, for the DSMA we show that the estimation of the constant locally introduces unreasonable peaks in some regions, a similar behaviour as with DSMA models in Navier-Stokes solvers.

INTRODUCTION

The aim of the current paper is to present our recent work on LES coupled with the Single Relaxation Time (SRT) LBM (Mohamad, 2011). Two LES models have been implemented, the DSMA (Premnath *et al.*, 2009) and WALE (Nicoud & Ducros, 1999), in our in-house solver AMROC (Deiterding, 2011) at the University of Southampton. Moreover, Adaptive Mesh Refinement (AMR) techniques are available to further improve the numerical efficiency of computations. In the next section, the theory describing LBM and the new LES models will be presented, together with the implementation of the force for the case of FHIT. After that, the section with the results will follow. Initially, FHIT DNS data will be shown, succeeded by FHIT LES, finishing with the discussion about the TGV case. Finally, we end the paper with a section about key-point conclusions and future work.

LATTICE BOLTZMANN METHOD

The SRT LBM finite difference scheme is usually decomposed into two steps. The first step is the streaming Eq. (1), where simply an exchange of information takes place among neighbour cells.

$$\check{f}_\alpha(\mathbf{x} + \mathbf{e}_\alpha \Delta t, t + \Delta t) = f_\alpha(\mathbf{x}, t) \tag{1}$$

The second step is the collision Eq. (2), a local per-cell calculation.

$$f_\alpha(\mathbf{x}, t + \Delta t) = \check{f}_\alpha(\mathbf{x}, t) + \frac{\Delta t}{\tau}(\check{f}_\alpha^{eq}(\mathbf{x}, t) - \check{f}_\alpha(\mathbf{x}, t)) \tag{2}$$

In the above equations, $\check{f}_\alpha$ are the intermediate values of the density distribution function after the streaming and before the collision. $\mathbf{x}$ are the coordinates of each cell and $\mathbf{e}_\alpha$ are the lattice velocities, which in case of the employed D3Q19 lattice model are 19. The time and time step are t and Δt, respectively. The single relaxation time τ can be estimated based on Eq. (3).

$$\tau = \frac{\nu + \Delta t c_s^2 / 2}{c_s^2} \tag{3}$$

Here, ν is the viscosity and c_s the speed of sound. A second-order truncated Maxwellian equilibrium distribution function f_α^{eq} Eq. (4) was used.

$$f_\alpha^{eq}(\mathbf{x}, t) = w_\alpha \, \rho \left[1 + \frac{\mathbf{e}_\alpha \cdot \mathbf{u}}{c_s^2} + \frac{(\mathbf{e}_\alpha \cdot \mathbf{u})^2}{2c_s^4} - \frac{\mathbf{u} \cdot \mathbf{u}}{2c_s^2} \right] \tag{4}$$

ρ denotes the density, $\mathbf{u}$ the velocity field and w_α the coefficients of the lattice model.

The connection between microscopic and macroscopic variables is achieved through the moments of the distribution functions f_α as in Eq. (5). Here, p is the pressure.

$$\rho(\mathbf{x},t) = \sum_\alpha f_\alpha(\mathbf{x},t) \qquad (5a)$$

$$\rho(\mathbf{x},t)u_i(\mathbf{x},t) = \sum_\alpha e_{\alpha i} f_\alpha(\mathbf{x},t) \qquad (5b)$$

$$p(\mathbf{x},t) = \rho(\mathbf{x},t)\, c_s^2 \qquad (5c)$$

External Force

For the realisation of the FHIT case, an external body force was applied. Its purpose is to charge the range of low wavenumbers $1 \leq \kappa_i \leq 2$ continuously with kinetic energy. The effect of the force was modelled by an extra term Eq. (6) added to the right-hand side of Eq. (2).

$$\frac{\Delta t \, w_\alpha(\mathbf{e}_\alpha \cdot \mathbf{F})}{c_s^2} \qquad (6)$$

The body force $\mathbf{F}$ is based on Abdel Kareem $et\ al.$ (2009).

$$
\begin{aligned}
F_x &= 2\rho A\left(\frac{\kappa_y \kappa_z}{|\kappa|^2}\right) G(\kappa_x, \kappa_y, \kappa_z, \phi) \\
F_y &= -\rho A\left(\frac{\kappa_x \kappa_z}{|\kappa|^2}\right) G(\kappa_x, \kappa_y, \kappa_z, \phi) \\
F_z &= -\rho A\left(\frac{\kappa_x \kappa_y}{|\kappa|^2}\right) G(\kappa_x, \kappa_y, \kappa_z, \phi)
\end{aligned}
\qquad (7)
$$

$G(\kappa_x, \kappa_y, \kappa_z)$ denotes the phase of the force.

$$G(\kappa_x, \kappa_y, \kappa_z) = \sin\left(\frac{2\pi x}{L}\kappa_x + \frac{2\pi y}{L}\kappa_y + \frac{2\pi z}{L}\kappa_z + \phi\right) \quad (8)$$

In the above equations, A is the acceleration due to the force, L the length of the domain, in this case 2π, $|\kappa|$ the magnitude of the vector of wavenumbers, and ϕ the random phase given by an equidistance distribution. Note that no effort was taken to correlate the values of ϕ in time.

LES in LBM

One way to incorporate LES into the LBM framework is through the alteration of the discrete relaxation time τ and its replacement by an effective discrete relaxation time $\tau^\star$ (Hou $et\ al.$, 1996). Consequently, the collision step Eq. (2) is replaced by Eq. (9).

$$\overline{f}_\alpha = \overline{\overline{f}}_\alpha + \frac{\Delta t}{\tau^\star}(\overline{\overline{f}}_\alpha^{\,eq} - \overline{\overline{f}}_\alpha) + \frac{\Delta t \, w_\alpha(\mathbf{e}_\alpha \cdot \overline{\mathbf{F}})}{c_s^2} \qquad (9)$$

The variable $\overline{f}_\alpha$ denotes the filtered values of the partial density distribution functions. The effective discrete relaxation time $\tau_L^\star$ Eq. (10) is computed locally per cell.

$$\tau^\star = \frac{(\nu + \nu_t) + \frac{c_s^2 \Delta t}{2}}{c_s^2} \qquad (10)$$

The notation ν_t is the eddy viscosity.

DSMA The implementation of the dynamic Smagorinsky model in the LBM is based on the work of Premnath $et\ al.$ (2009) and follows the idea of Germano $et\ al.$ (1991), including the modification of Lilly (1992).

For the case of the constant Smagorinsky (Smagorinsky, 1963) the eddy viscosity is computed based on Eq. (11).

$$\nu_t = (C\Delta)^2 |\overline{S}| \qquad (11)$$

The constant C is a user-defined value, Δ the spatial step and $|\overline{S}| = \sqrt{2\overline{S}_{ij}\overline{S}_{ij}}$ is the intensity of the strain rate. In the LBM framework the strain rate is related to a non-equilibrium momentum flux tensor Eq. (12).

$$\overline{Q}_{ij} = \sum_\alpha \mathbf{e}_{\alpha i}\mathbf{e}_{\alpha j}(\overline{f}_\alpha - \overline{f}_\alpha^{\,eq}) \qquad (12)$$

This tensor can be computed locally per cell avoiding the communication with neighbour cells. In that way, after some algebra, the effective relaxation time can be directly computed as in Eq. (13).

$$\tau^\star = \frac{\tau}{2} + \sqrt{\frac{\tau^2}{4} + \frac{C^2 \Delta^2 |\overline{Q}|}{2\rho c_s^4}} \qquad (13)$$

The variable τ is computed by Eq. (3).

For the DSMA, the difference is that the constant C in Eq. (13) is now estimated locally per cell, with the assistance of a test filter, in this case a trapezoidal one, applied on a coarser grid, and assuming scale invariance between the two filters. The interested reader can find more information in (Premnath $et\ al.$, 2009).

In theory (Lilly, 1992), an averaging in homogeneous directions and in time–for statistically steady flows–should be applied during the computation of C. However, in real engineering applications it is difficult to identify statistical homogeneity or steadiness, if they actually exist in the first place. This imposes the local computation of C, which can introduce unphysically peaks in some regions. To alleviate this issue the value of C is truncated as $0 \leq C \leq 0.23$.

WALE The idea in the WALE model is to replace the term $|\overline{S}|$ in Eq. (11) with a more advanced operator that can effectively handle the damping of the eddy viscosity in the vicinity of the wall (Nicoud & Ducros, 1999). The new operator is a function both of the strain rate S_{ij} and the rotation rate Ω_{ij}, as can be seen in Eq. (14).

$$OP_{WALE} = \frac{(\mathscr{J}_{ij}\mathscr{J}_{ij})^{\frac{3}{2}}}{(\overline{S}_{ij}\overline{S}_{ij})^{\frac{5}{2}} + (\mathscr{J}_{ij}\mathscr{J}_{ij})^{\frac{5}{4}}} \qquad (14)$$

The tensor $\mathscr{J}_{ij}$ is calculated as in Eq. (15).

$$\mathscr{J}_{ij} = \overline{S}_{ik}\overline{S}_{kj} + \overline{\Omega}_{ik}\overline{\Omega}_{kj} - \frac{1}{3}\delta_{ij}(\overline{S}_{mn}\overline{S}_{mn} - \overline{\Omega}_{mn}\overline{\Omega}_{mn}) \quad (15)$$

The notation δ_{ij} is the Kronecker delta. In this way, the eddy viscosity in Eq. (11) is replaced by Eq. (16).

$$\nu_t = (C_w \Delta)^2 OP_{WALE} \qquad (16)$$

The notation C_w denotes the constant of the model and is always equal to 0.5. To compute the two rates, central finite differences are used for the derivatives. Compared to the dynamic Smagorinsky model, the WALE model does not need truncation corrections.

RESULTS

In this section we will present the results of the two test cases, namely the FHIT and the TGV.

Forced Homogeneous Isotropic Turbulence

The computational domain for the FHIT test case was a cube of a 2π length with periodic boundary conditions in all three directions. The initial conditions were a zero velocity field and unit density everywhere. The value of the acceleration A of the force was 10^{-4} for all simulations, and the speed of sound was taken equal to the lattice one, i.e. $1/\sqrt{3}$. For a given resolution, the viscosity was used as a tuning parameter for the Re_λ that characterises this test case and is based on the Taylor length scale and the root mean square of the velocity field. However, the current implementation of the force was found to produce resolution depended Re_λ. After a transient time, the external energy due to the force equilibrates with the viscous dissipation and a statistically steady state is achieved, which can be eventually analysed. The choice of the transition time was made based on the examination of the evolution of the dissipation rate ε estimated in the Fourier space. The above circumstances enable a convenient extraction of the 3D energy spectra and their assessment. Therefore, the spectra were time-averaged over this steady state period. To achieve this endeavour, a Fourier transform per component of the velocity field was performed. The library FFTW (Frigo, 1999) was employed to deal with these transformations. All turbulent statistics were computed on fly.

To validate our DNS results, the model spectrum of Pope (2000) was employed. This model is the result of a compilation of a variety of experimental data. Its mathematical formula can be seen in Eq. (17).

$$E(\kappa) = C_K \varepsilon^{2/3} \kappa^{-5/3} f_L(\kappa L) f_\eta(\kappa \eta) \qquad (17)$$

C_K is the Kolmogorov constant equals to 1.5 and κ the wavenumber. The two functions $f_L(\kappa L)$ and $f_\eta(\kappa \eta)$ characterise the shape of the spectrum in the energy containing range and the dissipation range respectively. η is the Kolmogorov length scale and L a length describing the large eddies. For more information the interested reader can refer to (Pope, 2000).

DNS For the DNS results, a variety of resolutions were simulated, with the viscosity value $\nu = 5 \cdot 10^{-5}$, to monitor the behaviour of the AMROC-LBM implementation to deal with this elementary turbulent flow. Figure 1a presents the Kolmogorov spectra of the previously mentioned simulations. The deviation of the spectra of the two lowest resolutions in the energy-containing range is due to their lower values of Re_λ compared to the other two higher resolutions. It is important to mention that the deviation of the spectra from the model spectrum in this range is due to the application of the force to the lowest wavenumbers.

On the other hand, all four spectra are collapsing in higher wavenumbers, except for the highest ones, where
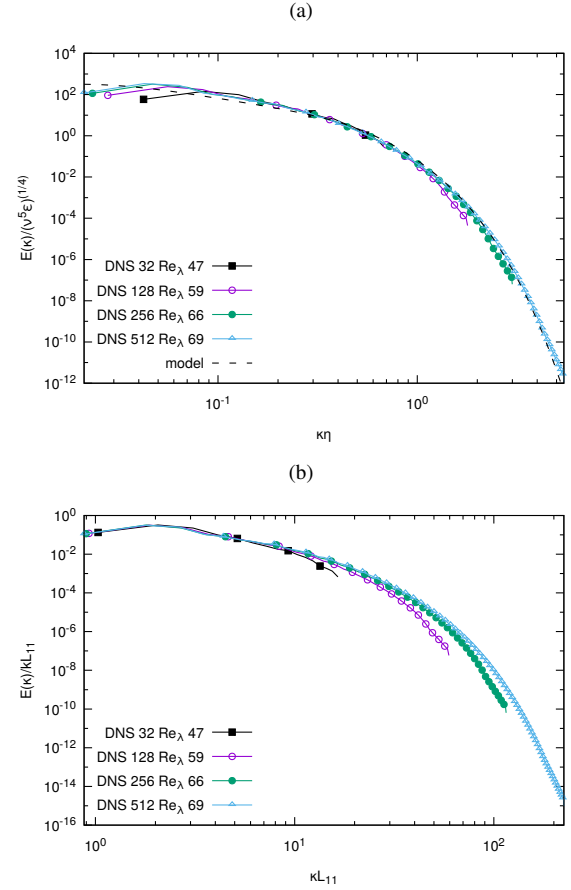
Figure 1: Time-averaged Kolmogorov energy spectra (a) and energy spectra normalised by the turbulent kinetic energy k and the integral length scale L_{11} (b) of LBM DNS (solid lines) and the model spectrum (dashed line) (Pope, 2000) for the viscosity $\nu = 5 \cdot 10^{-5}$.

the resolutions 128^3 and 256^3 exhibit a more dissipative behaviour. The lowest resolution is insufficiently resolved to exhibit a dissipation range. Moreover, the small peak that appears from the lowest resolution in the inertial sub-range is due to the force, and because of the low Re_λ the energy-containing range has merged with the inertial sub-range. The model spectrum was computed based on the values of the highest resolution, of 512^3 cells. However, under the Kolmogorov scaling of the spectra, the expected behaviour is their collapse in the dissipation range. Therefore, based on this model spectrum, for a fully resolved dissipation range a resolution of $\kappa_{max}\eta \geq 5$ is needed. This is in agreement with previous considerations for a value of $\kappa_{max}\eta \geq \pi$ (Peng et al., 2010).

Figure 1b shows the energy spectra normalised by the integral length scale L_{11} and the turbulent kinetic energy k, a suitable normalisation for comparison of the energy-containing range for different Re_λ. It is eminent that now all four spectra collapse in the low wavenumbers, with a small deviation for the lowest resolution for the previously mentioned reasons. This is an indication that, although this force produces resolution-dependent turbulent statistics, the simulated flows are similar.

Although all previous simulations have reproduced slopes close to $-5/3$ in the inertial sub-range, none of them

(a)

(b)
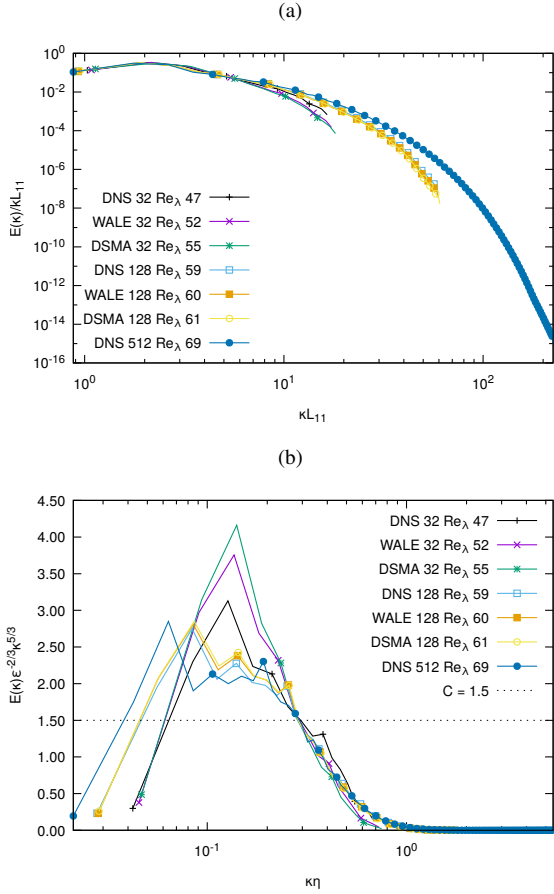
Figure 2: Time-averaged energy spectra normalised by the turbulent kinetic energy k and the integral length scale L_{11} (a) and compensated energy spectra (b) for LBM DNS and LES for the viscosity $\nu = 5 \cdot 10^{-5}$.

was able to compute a reasonable value for the Kolmogorov constant. The best estimate was for the resolution of 512^3 with a value of ~ 2. To further examine this issue, a simulation of 169 Re_λ with a resolution of 256^3 cells was conducted. Having examined its energy spectra, not shown here, we concluded that the simulation was under-resolved in the dissipation range. However, it was able to produce an inertial sub-range closer to the model spectrum with an estimated constant of 1.67.

LES Having obtained the results for DNS, we proceeded with LES to verify the newly implemented models. The inability of the force to produce resolution-independent statistical characteristics invalidates the use of Kolmogorov normalisation for the examination of the spectra for the LES. Therefore, the most suitable comparison of the spectra is the presentation employing a normalisation based on the turbulent kinetic energy k and the integral length scale L_{11}. Figure 2a shows these spectra of the two resolutions for the LES and their DNS counterparts. The DNS case of the highest resolution of 512^3 cells is also presented as a reference. Moreover, it is evident that the Re_λ is also related to the applied turbulent model. This discrimination is again reduced for higher resolution.

The DNS of the lowest resolution is under-resolved based on its value of $\kappa_{max}\eta$, while the 128^3 cells resolution has mainly under-resolved the dissipation range, based on

the results of the previous section. Apparently, all spectra collapse in the energy-containing range, under the logarithmic scaling of the axes, verifying that the LES models have not affected this range, as it was to be expected. The small deviation appearing in the spectra of the lowest resolution is again due to the low Re_λ and the application of the force. As far as the dissipation range is concerned, both LES of the lowest resolution exhibit a more dissipative behaviour compared to their DNS counterparts, while for the resolution of 128^3 cells there are no obvious deviations between DNS and LES.

Figure 2b presents the compensated spectra of the discussed simulations. First of all, it is eminent in this plot that for the lowest resolution, the inertial sub-range has merged with the energy-containing range, due to the low Re_λ. Moreover, the exaggerated peaks compared to the higher resolutions are due to the application of the force in this merged region. However, also the simulations of the resolution of 128^3 cells have overestimated the level in the inertial sub-range compared to the DNS of 512^3 cells, although this deviation is much smaller than for the lowest resolution.

As far as relative differences between DNS and LES cases are concerned, the LES models of the lowest resolution have computed higher energy in the lower wavenumbers compared to their DNS counterpart. On the other hand, the LES models have estimated a smoother slope in the dissipation range. On the contrary, these deviations are much smaller for the higher resolution of 128^3 cells. This is an indication of the employed LES models to adjust based on the resolution and be inactive in sufficient refined grids.

Another important observation is that the DSMA model has estimated larger values in the inertial sub-range compared to the WALE model for both resolutions. These discriminations are more evident in the lowest resolution.

Taylor Green Vortex

In the previous section about FHIT with LBM LES we have shown that there were some differences between DSMA and WALE models. To further examine their behaviours, the test case of the TGV was studied next. Again the domain was a cube with a length equals to $2\pi L$, where $L = 1$, and periodic boundary conditions were used at all sides. In this case there is no force and the flowfield was initialised as in Eq. (18).

$$u(\mathbf{x}, t_0) = U_0 \sin\left(\frac{x}{L}\right) \cos\left(\frac{y}{L}\right) \cos\left(\frac{z}{L}\right) \qquad (18a)$$

$$v(\mathbf{x}, t_0) = -U_0 \cos\left(\frac{x}{L}\right) \sin\left(\frac{y}{L}\right) \cos\left(\frac{z}{L}\right) \qquad (18b)$$

$$w(\mathbf{x}, t_0) = 0 \qquad (18c)$$

$$\rho(\mathbf{x}, t_0) = \rho_0 + \frac{\rho_0 U_0^2}{16 c_s^2}\left[\cos\left(\frac{2x}{L}\right) + \right.$$
$$\left. \cos\left(\frac{2y}{L}\right)\right]\left[\cos\left(\frac{2z}{L}\right) + 2\right] \qquad (18d)$$

(a)

(b)
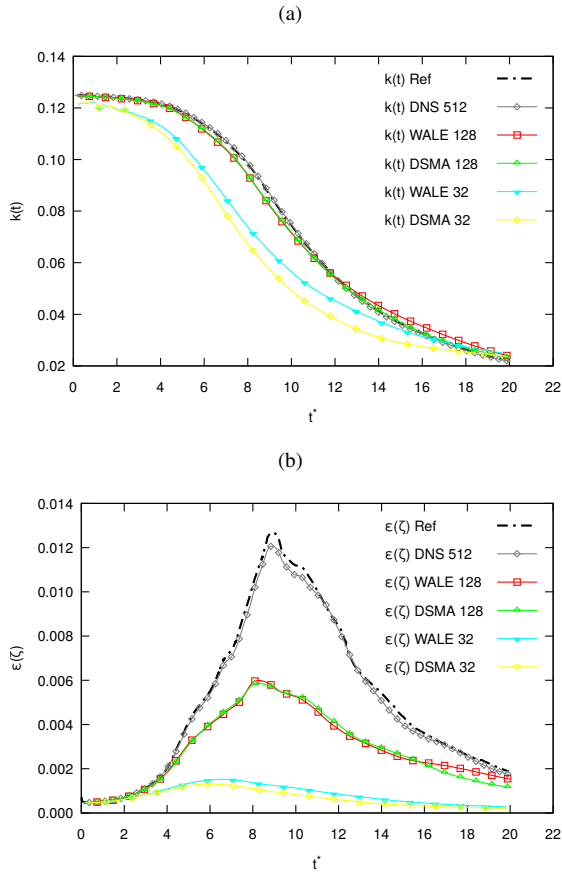
Figure 3: Evolution of kinetic energy (a) and dissipation based on enstrophy (b) in the domain for LBM DNS and LES for Re 1600 against the reference data of (DeBonis, 2013).

The applied values were $U_0 = 0.1$ and $\rho_0 = 1$. c_s was set to the lattice value of $1/\sqrt{3}$ and thus Ma ≈ 0.17. For the viscosity ν the value of $6.25 \ 10^{-5}$ was used, resulting in Re $= U_0 L / \nu = 1600$. The results are reported in non-dimensional form, as it is common for this test case.

The TGV test case imposes a variety of challenges to numerical methods and turbulence models. Until $t^* \approx 4$ the field is characterised by inviscid phenomena, such as stretching and rotation of big scale vortices. After this time and until $t^* \approx 9$, where is the peak of dissipation, the vortices are broken down to smaller scales and transition to turbulence takes place. This stage is then replaced by the decay of the kinetic energy by the small scales, and in the absence of an external force the flow will come to rest after sufficient time.

Figures 3a and 3b present the evolution of the domain averaged kinetic energy and the dissipation estimated from entrophy. The plots show the DNS data of the highest resolution of 512^3 cells, that has been achieved during this work, and two lower resolutions of the two LES models in question. For the resolution of 32^3 cells the simulations without a turbulence model did not converge. We adopt the reference data of DeBonis (2013) for comparison, where a 13-point dispersion-relation-preserving scheme after Bogey & Bailley was used. The resolution was 512^3 cells.

As for the kinetic energy, the LBM DNS was able to reproduce accurately the reference curve for all three stages. In the case of the dissipation, the LBM DNS pre-
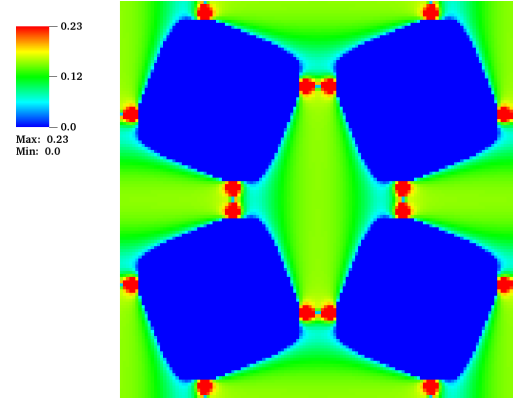
Figure 4: The Smagorinsky constant estimated at $t^* \approx 1$ from the DSMA model. The figure shows the slice at $z = \pi$ for the resolution of 128^3 cells.

dicted a slightly lower peak, while some discrepancies can be seen in the stage of the decay. This is an indication that a higher resolution should be used to match exactly with the 512^3 resolution of the reference. This is expectable since LBM, a second order method, is compared to a higher-order scheme.

On the other hand, the two LES of the 128^3 resolution captured the reference curves accurately for the first inviscid stage. This is an indication that the models were inactive when no small structures were present in the flow. In the breakdown stage, there is a steeper slope estimated by the LES models. Compared with a LBM DNS simulation of the same resolution (not shown here), we can conclude that the models were triggered incorrectly during this stage, dissipating part of the kinetic energy of the large scales. This also suggests that in regions of transition to turbulence the current models introduce more dissipation than they should. However, the DSMA was able to produce more accurate curves than the DNS in the decay stage. In contrary, the WALE model was unable to recover from the false activation during the second stage and over-estimated both the values of kinetic energy and dissipation compared to DSMA. Finally, both models have converged close to the end time, when the majority of kinetic energy has been dissipated, reducing the Re number and thus the small turbulent scales.

None of the LES at the lowest resolution was able to match any part of the reference kinetic energy. Moreover, oscillations can be detected in the initial stage of the curve as a result of inadequate resolution, which also increased the numerical dissipation. This excess of dissipation, even in the initial stage, depleted the kinetic energy of the large scales faster, leading to its premature reduction. In the second stage, the depletion of the large scales triggered the breakdown of smaller scales, reducing the peak value of dissipation in Fig. 3b. In contrary to the higher resolution LES, on coarse grids the WALE model behaved better than the DSMA.

To identify the reason of the pure behaviour of the DSMA, Fig. 4 shows the instantaneous values of C at $t^* \approx 1$ on the slice at $z = \pi$ of the 128^3 simulation for the DSMA. At this time, the field is still in the first inviscid stage, where big scale vortices are stretched, rotate and interact. It is obvious that the model was able to recognise the vortices, the four blue regions of reduced C values. In the rest of the domain, it returned a value around 0.1. However, in regions

where the vortices are about to interact, it overestimates the values, and it is only due to truncation at the value 0.23 that C remains in the reasonable range. Indeed, a simulation without the truncation restriction has calculated unreasonable values above 1. The situation was worse for the case of the lowest resolution, explaining the poor performance compare to the WALE model. Consequently, the source of this inaccuracy is because of the local estimation of C without taking into consideration homogeneous directions, which in this case are all three of them. We expect that applying the latter would result in more accurate results.

CONCLUSIONS AND FUTURE WORK

In this paper, we have verified our two newly implemented LBM LES models, DSMA and WALE, in our in-house solver AMROC by simulating FHIT and TGV in a periodic box. The absence of boundary conditions and the ability to easily estimate energy spectra and other statistical values in Fourier space make these two test cases ideal for testing turbulence models. For the case of FHIT, we have reported results for four resolutions of DNS up to 512^3 and two for LES up to 128^3 cells. In the case of TGV, we have shown a fine DNS simulation of 512^3 and two coarser LES up to 128^3.

As for the FHIT, we conclude that with the current employed force scheme the final achieved Re_λ is related to the grid resolution and the applied LES model. However, by scaling the spectra, it is still possible to compare different resolutions and models. The DNS results of FHIT have shown that for a fully resolved dissipation range a resolution of $\kappa_{max}\eta \geq 5$ is needed. This observation is based on the model spectrum of Pope (2000). Moreover, with the specific set-up, even the highest resolution was unable to estimate accurately the Kolmogorov constant in the inertial subrange. To test this further, a simulation with lower viscosity and thus higher Re_λ was run leading to an improved estimation, however the dissipation range appeared under-resolved.

On the other hand, the LES simulations of 128^3 resolution returned similar results with the DNS of the same resolution, indicating that they become inactive on a reasonably well resolved grid. On the contrary, at the lowest resolution, both turbulence models overestimated the peak of the spectra, while DSMA showed the largest difference. In the same time, they reduced the energy of the higher wavenumbers, resulting in a more dissipative flow field.

For the case of TGV, we have shown that a LBM DNS simulation on a 512^3 grid was comparable to a simulation of a higher-order finite difference scheme for the Navier-Stokes equations, giving testament of the low numerical dissipation of the LBM. For the resolution of 128^3 cells, both turbulent models were able to capture accurately the first inviscid stage, while they added extra dissipation incorrectly during the phase of the breakdown. The DSMA model, however, showed a recovery in the final decay stage with improved results compared to DNS. Finally, at the lowest resolution, none of the models was able to accurately capture the flow field, although the WALE model behaved slightly better. We showed that the reason for the poor accuracy of the DSMA is the locality of the estimation of the constant.

The two discussed test cases have verified the LES models for off-wall situations. A new verification campaign has been launched already for wall-bounded flows. More-over, a newly implemented wall function will alleviate the need of an excess number of cells close to the wall due to the use of Cartesian grids. Finally, all models will be ensured to also work flawlessly with the AMR capability of the solver.

REFERENCES

Abdel Kareem, Waleed, Izawa, Seiichiro, Xiong, Ao-Kui & Fukunishi, Yu 2009 Lattice Boltzmann simulations of homogeneous isotropic turbulence. *Computers & Mathematics with Applications* **58** (5), 1055–1061.

DeBonis, James 2013 Solutions of the Taylor-Green Vortex Problem Using High-Resolution Explicit Finite Difference Methods. In *51st AIAA Aerospace Sciences Meeting including the New Horizons Forum and Aerospace Exposition*. Grapevine (Dallas/Ft. Worth Region), Texas: American Institute of Aeronautics and Astronautics.

Deiterding, Ralf 2011 Block-structured Adaptive Mesh Refinement - Theory, Implementation and Application. *ESAIM: Proceedings* **34**, 97–150.

Frigo, Matteo 1999 A fast Fourier transform compiler. In *ACM Sigplan Notices*, , vol. 34, pp. 169–180. ACM.

Germano, Massimo, Piomelli, Ugo, Moin, Parviz & Cabot, William H. 1991 A dynamic subgridscale eddy viscosity model. *Physics of Fluids A: Fluid Dynamics* **3** (7), 1760–1765.

Hou, S., Sterling, J., Chen, S. & Doolen, G. D. 1996 A lattice Boltzmann subgrid model for high Reynolds number flows. In *Pattern formation and lattice gas automata* (ed. A. T. Lawniczak & R. Kapral), , vol. 6, pp. 151–166. Fields Inst Comm.

Lilly, D. K. 1992 A proposed modification of the Germano subgridscale closure method. *Physics of Fluids A: Fluid Dynamics* **4** (3), 633–635.

Mohamad, A. A. 2011 *Lattice Boltzmann method: fundamentals and engineering applications with computer codes / A. A. Mohamad*. London ; New York: Springer.

Nicoud, F. & Ducros, F. 1999 Subgrid-scale stress modelling based on the square of the velocity gradient tensor. *Flow, Turbulence and Combustion* **62**, 183–200.

Peng, Yan, Liao, Wei, Luo, Li-Shi & Wang, Lian-Ping 2010 Comparison of the lattice Boltzmann and pseudo-spectral methods for decaying turbulence: Low-order statistics. *Computers & Fluids* **39** (4), 568–591.

Pope, S. B. 2000 *Turbulent flows*. Cambridge; New York: Cambridge University Press.

Premnath, Kannan N., Pattison, Martin J. & Banerjee, Sanjoy 2009 Dynamic subgrid scale modeling of turbulent flows using lattice-Boltzmann method. *Physica A: Statistical Mechanics and its Applications* **388** (13), 2640–2658.

Smagorinsky, J. 1963 General circulation experiments with the primitive equations, I: The basic experiment. *Monthly Weather Review* **91** (3), 99–164.